OXYGEN CONTROL DURING MANUFACTURING OF CeS-BASED GRAIN REFINERS FOR STEEL

Erlend Nordstrand & Øystein Grong
Norwegian University of Science and Technology, Norway

Casper Van der Eijk & Sean Gaal
SINTEF Materials and Chemistry, Norway

ABSTRACT

In the present investigation the conditions for cerium oxide and oxysulphide formation during manufacturing of CeS-based grain refiners for steel have been examined. The small vacuum furnace used in these laboratory experiments is equipped with a graphite heating element, where both the temperature-time programme and the partial pressure of oxygen can be accurately controlled and monitored throughout the melting trials. The results from the optical and electron microprobe examinations of the as-solidified samples show that the liquid Ce-S-Fe-Al melt is prone to oxidation up to about 1600 to 1800˚C before the graphite heating element starts to act as an effective oxygen scavenger. The oxidation leads to conversion of CeS to Ce_2O_2S, which is an undesirable microconstituent in the grain refiners. In practice, the problem can be overcome by the use of rapid heating of the melt, which in the present small-scale laboratory experiments needs to be as high as 1000˚C/min in order to kinetically suppress the oxygen absorption from the shielding gas.

INTRODUCTION

Cerium-treatment is widely used for inclusion engineering and grain size control of steel [1, 2, 3]. This is because cerium will form complex oxides and sulphides when added to liquid steel, with the ability to nucleate different types of ferrite during subsequent steel processing in the solid state [4]. However, a major problem with the use of pure cerium as an alloying element is that the element is not protected by a stable oxide layer, meaning that it will gradually disintegrate in contact with air. This disintegration is believed to be related to an intermediate formation of Ce_2O_3 on the cerium surface. The Ce_2O_3 oxide will subsequently be converted into the more stable CeO_2 oxide, which continuously destroys the protective film and allows the oxidation process to proceed in a destructive manner [5].

Also during manufacturing of CeS-based grain refiners for steel, which in the present case involves melting, superheating and quenching of a premixed Ce+FeS_2+Al blend [6], the combination of a high oxygen affinity and the lack of protection from a dense surface oxide layer creates serious problems. In practice, it is extremely difficult to achieve sufficiently low levels in the surrounding gas atmosphere which will eliminate the oxidation of liquid cerium. One option is to use a vacuum furnace equipped with a graphite heating element. Following refilling with a high-purity shielding gas (e.g. argon) such heating elements can protect the molten cerium from oxidising at temperatures approaching 2000˚C because carbon will be in control of the oxygen level at these temperatures [7]. Still cerium will be unprotected within an intermediate temperature range, where its affinity to oxygen is higher compared with carbon [8]. This, in turn, requires the use of rapid heating of the melt in order to avoid severe oxidation of cerium due to reactions with the surrounding gas atmosphere.

The main objective of the present investigation is to clarify the conditions under which CeS-based grain refiners can be manufactured without excessive cerium oxide formation during liquid metal processing. The experiments will be carried out in a small laboratory furnace equipped with a graphite heating element, where both the temperature-time programme and the partial pressure of oxygen can be accurately controlled and monitored throughout the melting trials. Optical and electron microscopy is then employed to characterise the different phases which form following heating and cooling of the samples. At the same time their thermodynamic stability at elevated temperatures is evaluated and compared based on calculations of the critical oxygen partial pressure for cerium oxide and cerium oxysulphide formation.

METHODOLOGY

Vacuum Furnace

Figure 1 shows a schematic illustration of the vacuum furnace used in the melting experiments. This furnace is originally designed for in-situ wetting angle measurements. As a consequence, the furnace is only equipped with a sample holder capable of heating substrates/crucibles with an outer diameter of 10 mm. Small tantalum crucibles were therefore machined to fit this sample holder. Tantalum has good refractory properties, is easy to machine and has a low solubility in contact with liquid cerium.

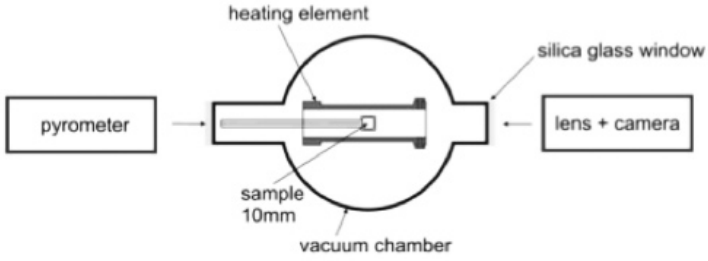

Figure 1: Schematic illustration of the vacuum furnace, which consists of an outer vacuum chamber, a graphite heating element and a sample holder. A camera system and pyrometer are mounted on the outside on each side of the furnace

To protect the sample from oxidising the vacuum chamber was constantly flushed with high purity argon during the experiments. The argon flowing out of the furnace passes through a zirconia oxygen sensor (Sensotec RX2100), which measures the partial pressure of oxygen. The RX2100 sensor can measure a partial pressure of oxygen from 1 to 10-26 atm with an accuracy of +/- 1% [9]. When starting the argon flushing, the oxygen partial pressure will after a certain period of time stabilize itself at around 10^{-15} atm. Such low oxygen levels are obtainable because the argon passes through a separate furnace, containing heated magnesium, before entering the vacuum furnace.

The heating element is constructed of graphite, as are all the other heated parts of the furnace. A calibrated pyrometer, with an operating temperature range from 900-2400°C, continuously measures the temperature of the crucible. In-situ photography of the crucible is also possible during the experiments, as shown in Figure 2.

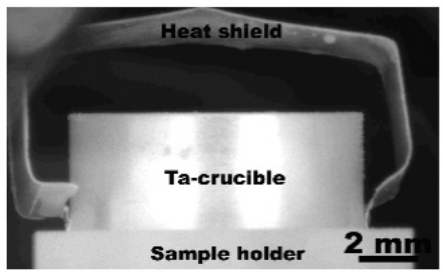

Figure 2: In-situ photography of the tantalum crucible during heating

Charge Materials

The charge materials used in the melting experiments are Ce, FeS_2 and Al. These have a purity of at least 99.9% and were obtained from different commercial manufacturers. To avoid oxygen contamination of the charge materials, an argon-filled glove box with oxygen and humidity levels <<0.1 ppm was used for storage. All charging of materials into the tantalum crucibles was done inside the glove box.

Melting Experiments

In order to evaluate the extent of oxygen absorption during superheating of the melt up to 2000°C, two different heating rates were employed, i.e., 60 and 1000°C/min. In both cases the blend of Ce+FeS_2+Al was adjusted to achieve the target composition of 86.8 wt%

Ce, 6 wt% S, 5.2 wt% Fe and 2 wt% Al. Note that the aluminium is added to promote Ce_3Al formation in the as-solidified samples, since previous experiments have shown that this level is sufficient to stabilise cerium during subsequent storage in air at room temperature.

Microscopy

Standard metallographic techniques were employed to prepare cross section samples for microstructure characterisation. Because Ce corrodes vigorously in water, wet grinding was carried out using an alcohol based lubricant. In the light microscope the microstructure was readily revealed without etching. Optical examination was preformed using a conventional Zeiss reflecting light microscope. In addition, phase characterisation was done employing backscatter electron (BSE) imaging and wavelength dispersive X-ray spectrometry (WDS). These investigations were carried out in a JEOL JXA-8500F electron microprobe using an acceleration voltage of 15 keV and a probe current of 30 nA.

RESULTS

Measured Oxygen Levels inside the Vacuum Furnace during Heating and Cooling

Figure 3 shows plots of the recorded crucible temperature and the measured level inside the vacuum furnace as a function of time during a typical rapid heating cycle (i.e., ~1000˚C/min).

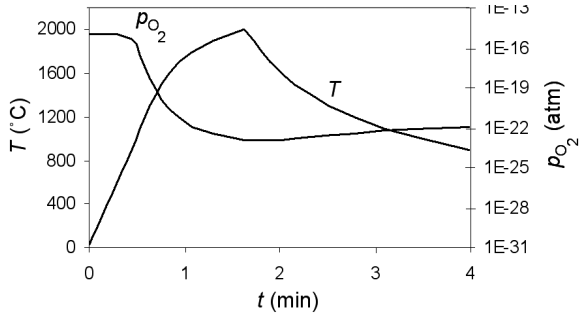

Figure 3: Graphical representations of the measured crucible temperature T and the partial pressure of oxygen inside the vacuum furnace during a typical rapid heating cycle (~1000˚C/min)

As expected, the use of a separate gas cleaning system implies that the partial pressure of oxygen in the Ar shielding gas is reduced to about 10 -15 atm before it is allowed to enter the vacuum furnace. During initial heating of the sample, p_{O2} starts to decrease as the temperature inside the furnace increases, reaching a lower threshold of about 10-22 atm after about 1 min when T > 1800˚C. This oxygen level is then largely maintained throughout the remaining melting experiment, also when the crucible temperature drops again below 1000˚C on subsequent cooling.

Phase Characterisation

Figures 4 (a) and (b) show two BSE images of the as-solidified microstructures taken at high magnification.

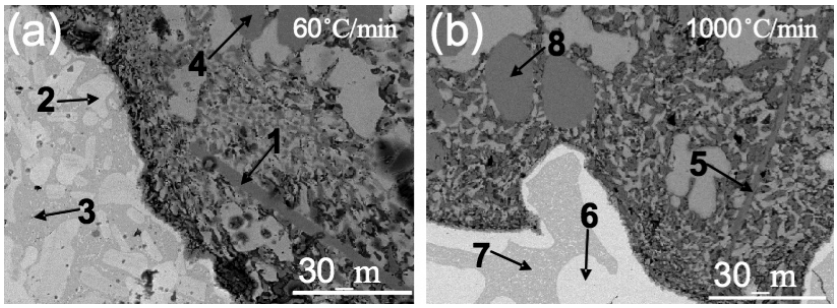

Figure 4: Two BSE images showing the as-solidified microstructures at high magnification. The applied heating rates of the samples in image (a) and (b) are 60 and 1000°C/min, respectively. The arrows in the images indicate the position of the eight point analyses reported in Table 1.

The eight WDS point analyses shown in Table 1 were carried out at the surface positions indicated by the arrows in the two electron micrographs. In the point analyses 1, 5, 4 and 8 the ratio between the constituent elements corresponds to the two intermetallic phases Ce_2O_2S and CeS, respectively. In addition, separate phases of Ta and Fe are present, as indicated by the point analyses 2, 3, 6 and 7. This shows that some reaction has occurred between Fe dissolved in the melt and the Ta crucible during heating and cooling.

Table 1: WDS point analyses of various phases detected in the as-solidified samples. Point analyses No. 1-4 refer to the sample being heated at 60°C/min, whereas point analyses No. 5-8 refer to the sample being heated at 1000°C/min. The numbers are given in at%.

No.	Al	O	S	Ta	Ce	Fe	Total
1	0.0	39.5	19.2	0.1	41.0	0.2	100.0
2	0.9	6.2	0.0	85.7	0.6	6.6	100.0
3	2.4	4.1	0.0	56.7	0.5	36.3	100.0
4	0.0	2.0	47.3	0.0	50.6	0.1	100.0
5	0.0	40.9	18.7	0.0	40.3	0.1	100.0
6	0.9	5.6	0.3	84.0	0.4	8.8	100.0
7	1.9	6.9	0.1	53.0	0.9	37.2	100.0
8	0.1	2.8	46.0	0.0	51	0.1	100.0

Figures 5 (a) and (b) show optical micrographs of the same surface areas being displayed previously in Figures 4 (a) and (b). These are taken at low magnification. The Ce_2O_2S and CeS phases, which have been identified by point analyses in Table 1, can also be recognised in these optical images by their morphologies, as shown by the arrows in Figure 5. A qualitative comparison between the two micrographs in Figure 5 reveals that the fraction of Ce_2O_2S needles in image (a) is significantly higher than in image (b). At the same time the fraction of CeS particles is seen to be highest in image (b). These results show that oxygen absorption from the surrounding shielding gas, as affected by the applied heating rate, is critical in the sense that it affects the phase balance between Ce_2O_2S and CeS in the as-solidified samples.

Moreover, it is evident from Figure 5 that the Ta-Fe reaction has mainly occurred at the interface between the Ta crucible and the melt. Apparently, the Ta-Fe compound formation is most severe in the sample being heated at 60°C/min, suggesting that this is also a kinetic-controlled reaction.

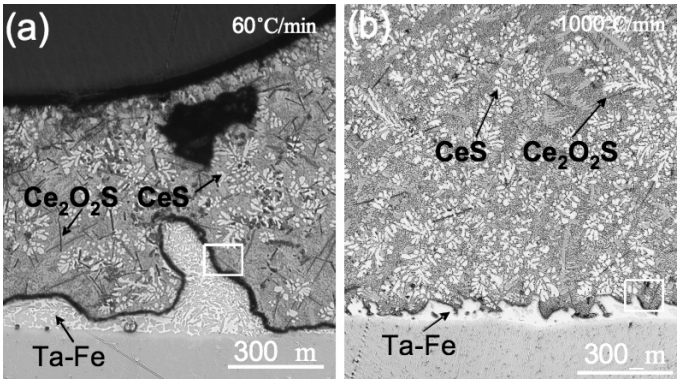

Figure 5: Optical images of the as-solidified microstructures taken at low magnification. The applied heating rates of the samples in image (a) and (b) are 60 and 1000°C/min, respectively. The different phases which previously have been identified by WDS point analyses are indicated by the arrows in the micrographs.

DISCUSSION

In the following, the conditions for oxidation formation during manufacturing of CeS-based grain refiners for steel will be discussed more in detail, starting with an analysis of factors controlling the partial pressure of oxygen in the shielding gas at elevated temperatures.

Oxygen Purification Efficiency of Graphite

As shown previously Figure 3, the oxygen level inside the furnace remains unchanged up to about 800°C during heating. At higher temperatures drops by several orders of magnitude. Similar oxygen profiles have been reported for resistant-heated graphite furnaces used for atomic absorption spectrometry [10, 11]. In the latter case it is believed that the oxygen purification effect is caused by the following reaction [12]:

$$O_2(g) + 2C(s) = 2CO(g) \quad (1)$$

At low temperatures this reaction is kinetically limited by a high activation energy for formation of carbon-oxygen bonds at the graphite surface. But at higher temperatures the activation energy is greatly reduced, which means that the graphite becomes increasingly reactive towards oxygen [13]. Under such conditions the oxygen partial pressure is controlled by the rate at which the oxygen can diffuse towards the graphite surface, allowing p_{O2} to drop below 10^{-22} atm, as observed in the present investigation.

It should be noted that the physical meaning of such a low p_{O2} in terms of numbers of O_2 molecules inside the furnace is that the oxygen content is practically zero. This means that any O_2 molecules entering the furnace chamber will immediately be picked up by the graphite heating element. It is therefore reasonable to assume that the oxidation of cerium will mainly occur during heating in the temperature range below, say, 1600 to 1800°C, p_{O2} where is significantly higher than 10^{-22} atm.

Critical Oxygen Partial Pressure for Cerium Oxide and Cerium Oxysulphide Formation

During heating of cerium and sulphur in the presence of oxygen, the following three oxidation reactions may occur:

$$2Ce + O_2(g) + S = Ce_2O_2S \quad (2)$$

$$2Ce + 1.5O_2(g) = Ce_2O_3 \quad (3)$$

$$Ce + O_2(g) = CeO_2 \quad (4)$$

By utilizing appropriate input data for the Gibbs energy of cerium oxide and oxysulphide formation [7], the critical needed to form Ce_2O_2S, Ce_2O_3 and CeO_2 as a function of temperature has been calculated. In Figure 6 these values have been superimposed on the measured temperature and oxygen profiles shown previously in Figure 3.

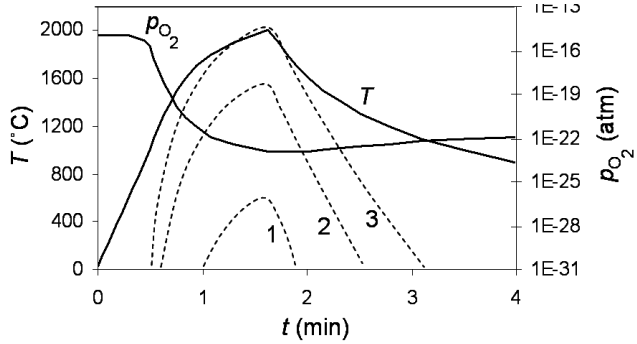

Figure 6: Graphical representation of the measured temperature T and the partial pressure of oxygen p_{02} inside the vacuum furnace during a typical rapid heating cycle (~1000°C/min). Plots 1-3 show the corresponding partial pressure of oxygen needed to form Ce_2O_2S, Ce_2O_3 and CeO_2, respectively at different temperatures. These calculations are done using thermodynamic input data from [7].

As the time evolves and the temperature inside the furnace increases, the stability of the different oxides decreases correspondingly, as shown in Figure 6. When the temperature exceeds 1800°C the measured oxygen level inside the furnace drops below the partial pressure needed to form CeO_2 and Ce_2O_3. On the other hand, Ce_2O_2S may still form and hence, Ce_2O_2S is the most likely oxide phase to be found in the as-solidified samples. This agrees well with the WDS point analyses in Table 1.

Kinetics of Oxygen Absorption during Heating

Figure 7 shows a schematic drawing of the Ta crucible inside the vacuum furnace, where the partial pressure gradient of oxygen between the bulk gas phase p^{b}_{O2} and the bare cerium surface p^{s}_{O2} also is indicated.

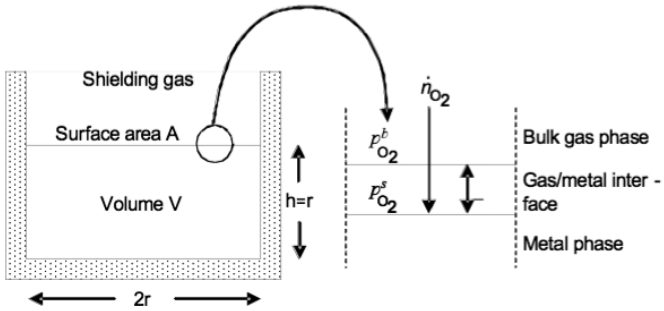

Figure 7: Idealised kinetic model for absorption of oxygen during heating of the Ce-melt inside the vacuum furnace

Referring now to this figure, the molar flux $\dot{n}_{O2}$ of O_2 (in mol s^{-1}) across the stagnant gaseous boundary layer of thickness δ (in m) at the gas/metal interface can be expressed as [14]:

$$\dot{n}_{O_2} = \frac{dn_{O_2}}{dt} = \frac{D_{O_2} A}{dRT}\left(p^b_{O_2} - p^s_{O_2}\right) = k_{O_2} A\left(p^b_{O_2} - p^s_{O_2}\right) \tag{5}$$

where D_{O2} is the oxygen diffusivity (in m^2 s^{-1}), R is the universal gas constant (in m^3 atm K^{-1} mol^{-1}), T is the absolute temperature (in K) and k_{O_2} is the overall mass transfer coefficient of oxygen (in mol m^{-2} s^{-1} atm^{-1}).

Based on Equation (5) it is possible to obtain a simple expression for the molar concentration of atomic oxygen per unit volume of the Ce-melt C_O (in mol m^{-3}). Taking the surface area to volume A/V ratio of the Ce-melt equal to $1/r$ (where r is the radius of the cylindrical Ta crucible), we arrive at:

$$C_O = 2\frac{A}{V}\int_0^t k_{O_2}\left(p^b_{O_2} - p^s_{O_2}\right)dt = \frac{2}{r}\int_0^t k_{O_2}\left(p^b_{O_2} - p^s_{O_2}\right)dt \tag{6}$$

In the limiting case, where both k_{O_2}, p^{b}_{O2} and p^{s}_{O2} are constant and independent of temperature (and thus time), the integral reduces to:

$$C_O = \frac{2}{r} k_{O_2}\left(p^b_{O_2} - p^s_{O_2}\right)t \tag{7}$$

Equation (7) shows, in an explicit manner, the main variables that come into play and contribute to the absorption of oxygen during heating of cerium inside the vacuum furnace. In general, the use of a small Ta crucible implies that the oxygen pick-up will be favoured by a large A/V ratio of the Ce-melt. Under such conditions oxygen purification of the shielding gas becomes extremely important. It follows that gas cleaning, employing heated magnesium powder in combination with the protection provided by the graphite heating element, are sufficient to avoid extensive oxidation at temperatures above, say, 1600 to 1800°C. Still, cerium is unprotected within an intermediate temperature range where $p^{b}_{O2} >> p^{s}_{O2}$. This, in turn, requires the use of rapid heating of the melt in order to minimise oxygen pick-up from the surrounding gas atmosphere. In the present small-scale laboratory experiments a heating rate of about 1000°C/min is required to limit the conversion of CeS to Ce_2O_2S, which is an undesirable microconstituent in the grain refiners.

CONCLUSIONS

The basic conclusions that can be drawn from this investigation are as follows:

- In a pure metallic form, cerium is a difficult element to handle because it will readily oxidise and disintegrate at room temperature in contact with air. Thus, in order to avoid oxygen contamination of the cerium both charging and storage of the material must be done inside a glove box under the shield of an inert gas.
- Also during manufacturing of CeS-based grain refiners for steel, the high reactivity of cerium towards oxygen creates serious problems. In particular, in small-scale melting trials involving the use of cerium oxygen, purification of the shielding gas becomes extremely important. Experiments carried out inside the laboratory vacuum furnace show that gas cleaning, employing heated magnesium powder in combination with the protection provided by the graphite heating element, are sufficient to prevent cerium from oxidising at temperatures above, say, 1600 to 1800˚C.
- However, at intermediate temperatures cerium is unprotected and will readily oxidise, unless the reaction is kinetically suppressed through the use of rapid heating. For example, when a blend of Ce+FeS_2+Al is melted inside a Φ8 mm Ta crucible, a heating rate of about 1000˚C/min is required to limit the conversion of CeS to Ce_2O_2S. The cerium oxysulphide is the thermodynamic stable phase in the presence of oxygen and sulphur, but is an undesirable microconstituent in the grain refiners and should therefore be avoided.

ACKNOWLEDGMENTS

The authors would like to thank Mr. Morten Peder Raanes at the Department of Materials Science & Engineering, NTNU, Trondheim, Norway for carrying out the electron microprobe examinations. Also, the financial support provided by the Norwegian Research Council through the DISvaDRI project is gratefully acknowledged.

REFERENCES

Ohmori, A., Kawabata, F. & Amano K. (2000). *Low-Carbon Steels Microalloyed for High Tensile Strength, and Suitable for Welding with High Heat Input*. Patent EP 1 035 222 A1. [1]

Grong, Ø. & Klevan, O. S. (2001). *Method for Grain Refining of Steel, Grain Refining Alloy for Steel and Method for Producing Grain Refining Alloy*. Patent WO 2001/57280. [2]

Grahle, P., Ruch, R. & Stiegeler, H. (2005). *Method for the Production of High-Alloy Cast Steel Material Having a Fine Grain Structure*. Patent WO 2005/026396. [3]

Thewlis, G. (2006). *Effect of Cerium Sulphide Particle Dispersions on Acicular Ferrite Microstructure Development in Steels*. Materials Science and Technology, Vol. 22, pp. 153-166. [4]

Loriers, J. (1949). *The Oxidation of Cerium and Lanthanum*. Compt. rend., Vol. 229, pp. 547-549. [5]

Grong, Ø., Kolbeinsen, L., Van der Eijk, C. & Tranell, G. (2006). *Microstructure Control of Steels through Dispersoid Metallurgy using Novel Grain Refining Alloys*. ISIJ International, Vol. 46, pp. 824-831. [6]

Kubaschewski, O. & Alcock, C. B. (1979). *Metallurgical Thermochemistry*. Pergamon Press, Sydney. [7]

Wilson, W. G., Kay, D. A. R. & Vahed, A. (1974). Use of Thermodynamics and Phase Equilibriums to predict the Behavior of the Rare Earth Elements in Steel. *Journal of Metals*, Vol. 26, pp. 14-23. [8]

Sensotec RX2100. (2004). http://www.cambridge-sensotec.co.uk/pdfs/Rapidox_2100_Instruction_Manual_version_1.5.pdf. [9]

L'vov, B. V. & Ryabchuk, G. N. (1982). *A New Approach to the Problem of Atomization in Electrothermal Atomic Absorption Spectrometry*. Spectrochimica Acta. B., Vol. 37B, pp. 673-684. [10]

Chang, S. B., Chakrabarti, C. L., Huston, T. J. & Byrne, J. P. (1985). *Estimation of Partial Pressure of Oxygen inside the Graphite Furnace used for Atomic Absorption Spectrometry*. Fresenius Z. Anal. Chem., Vol. 322, pp. 567-573. [11]

Sturgeon, R. E., Siu, K. W. M. & Berman, S. S. (1984). *Oxygen in the High-temperature Graphite Furnace*. Spectrochimica Acta. B. 39B, pp. 213-224. [12]

Blanchard, A. (2003). Appendix 2. *The Thermal Oxidation of Graphite. Irradiation Damage in Graphite due to fast Neutrons in Fission and Fusions Systems*. IAEA-TECDOC-1154, pp. 207-213. [13]

Rosenqvist, T. (1983). P*rinciples of Extractive Metallurgy*. 2nd Ed. McGraw-Hill International Book Company, Singapore. [14]